Dissolution kinetics of garnierites from the Falcondo Ni-Laterite deposit (Dominican Republic) under acidic conditions

Cristina Villanova-de-Benavent [a,*], Jordi Cama [b], Josep M. Soler [b], Cristina Domènech [a], Salvador Galí [a], Joaquín A. Proenza [a]

[a] Departament de Mineralogia, Petrologia i Geologia Aplicada, Facultat de Ciències de la Terra, Universitat de Barcelona (UB), Martí i Franquès s/n, 08028, Barcelona, Spain
[b] Institute of Environmental Assessment and Water Research (IDAEA), CSIC, Jordi Girona 18-26, 08034, Barcelona, Catalonia, Spain

ARTICLE INFO

ABSTRACT

In this study we tested the dissolution kinetics of three garnierite types (serpentine-, talc- and sepiolite-dominated) at pH of 3 and 5 and room temperature by means of flow-through experiments. The samples selected for the study cover a wide range of mineralogical composition (X_{talc}, between 0.34 and 0.78) and Ni content (between 0.8 and 2.4 atoms per formula unit Ni).

The variation in the output concentrations of Ni, Mg and Si over time showed a depletion of Si (tetrahedral cation) and Ni (octahedral cation), resulting in non-stoichiometric dissolution reactions. Since the release of Mg was faster than that of Ni and Si, the overall dissolution rates were based on its release (R_{Mg}) and normalised to the final specific surface area.

The steady-state dissolution rates of these garnierites decreased with increasing pH, and no correlation between R_{Mg}, talc content and Ni/Si ratio was found. The dissolution rate-pH dependence was calculated with the equation $R_{Mg} = k_{H^+} \times a_{H^+}^{n_{H^+}}$ (R_{Mg} is the Mg-based dissolution rate, k_{H^+} is the dissolution rate constant and $a_{H^+}^{n_{H^+}}$ is the dependence on the activity of H^+), with k_{H^+} and n_{H^+} equal to $-10^{-11.3}$ and 0.25 (serpentine-dominated experiments), $-10^{-12.1}$ and 0.19 (talc-dominated experiments), and $-10^{-11.6}$ and 0.25 (sepiolite-falcondoite). The provided rate laws for the different types of garnierites will allow a more accurate interpretation and understanding of the formation of these weathering profiles through the implementation of geochemical reactive transport modelling. Further work should include integrating data from experiments under neutral or slightly alkaline conditions.

1. Introduction

Garnierites are a group of fine-grained Ni–Mg-phyllosilicates including serpentine, kerolite (a mineral with talc structure and additional water), sepiolite, smectite and chlorite, often occurring as poorly crystalline mixtures (e.g. Brindley and Hang, 1973). Garnierites are the highest-grade nickel ores found in hydrous silicate-type Ni-laterite deposits and have been extensively studied in New Caledonia (e.g. Wells et al., 2009; Fritsch et al., 2015; Cathelineau et al., 2016), Indonesia (e.g. Fu et al., 2014), Australia (e.g., Putzolu et al., 2020b), and the Dominican Republic (Tauler et al., 2009; Galí et al., 2012; Villanova-de-Benavent et al., 2014, 2016, 2019; Roqué-Rosell et al., 2017) in recent years.

The genesis of garnierites is still matter of scientific debate. However,

the most accepted model inferred that these complex aggregates of Ni-phyllosilicates precipitate as open space infillings (such as in fractures, joints and fault planes) from Si- and Ni-saturated solutions percolating downwards through the lowermost part (i.e. saprolite and saprock) of the laterite profile (e.g. Freyssinet et al., 2005). During tropical weathering of an ultramafic rock, the primary ferromagnesian silicates, containing low levels of Ni, are altered to Ni-enriched secondary phases, such as Ni-bearing serpentines (Freyssinet et al., 2005; Villanova-de-Benavent et al., 2017; Tauler et al., 2017; Putzolu et al., 2020a) and Ni-bearing Fe oxyhydroxides (Freyssinet et al., 2005; Roqué-Rosell et al., 2010; Domènech et al., 2017; Santoro et al., 2021). During this process, Mg is solubilised and leached out of the weathering profile, whereas Fe and Ni are retained in goethite in the upper oxide horizon (e. g. Butt and Cluzel, 2013). This Ni, after its residual enrichment in the

upper part of the profile, may subsequently be leached by percolating acidic solutions and transported to deeper levels in the profile following the so-called *per-descensum* model (e.g. Freyssinet et al., 2005; Butt and Cluzel, 2013). The above process leads to an initial Ni fixing into serpentine (Pelletier, 1996). Once the serpentine minerals are saturated, the excess Ni precipitates as garnierites in open spaces (e.g. Freyssinet et al., 2005). Recent studies proposed that garnierites are precipitated in a tectonically active regime in which Ni is reconcentrated through recurrent weathering–uplift–erosion cycles (Villanova-de-Benavent et al., 2014). The formation of the ore occurs in successive stages becoming progressively enriched in Ni and Si (Galí et al., 2012).

The Eh, pH, and chemical composition of permeating water within the laterite profile play a major role in defining the stability of Ni-bearing minerals (e.g. Trescases, 1973). Concerning reaction rates, a first study was performed by Soler et al. (2008) on the Loma de Hierro deposit (Venezuela). The main finding of this study was that the garnierite dissolution rate decreases with increasing pH under acidic conditions. Furthermore, the dissolution process was congruent at pH > 5 and incongruent at pH < 5. This contrasting behaviour resulted from the different contribution of serpentine and talc to the total dissolution rate (the serpentine component tends to dissolve faster under more strongly acidic conditions).

Previous studies on Dominican Republic garnierites outlined the mineralogical and chemical complexity of these Ni-phyllosilicates and ascribed the variability to the contribution of serpentine-, talc- (kerolite) and sepiolite-like phases (e.g. Villanova-de-Benavent et al., 2014). In this study, the term talc will be used to describe the kerolite-like phases. Both in Falcondo and in Loma de Hierro, Ni has been found to have a large affinity for the talc-like phases (e.g. Soler et al., 2008; Galí et al., 2012; Villanova-de-Benavent et al., 2016). Furthermore, in an Al-free system, such as in the Falcondo mining district (Dominican Republic), the stability of serpentine-, talc- and sepiolite-like garnierites is controlled by the activity of silica (Galí et al., 2012). In particular, the increase of the Si activity during the lateritisation process triggers the precipitation of Ni-phyllosilicates as a succession of mineral phases progressively enriched in Ni and Si. Accordingly, the first garnierites to precipitate are serpentine-like, followed by talc-like and sepiolite–like (sepiolite-falcondoite) (Galí et al., 2012; Villanova-de-Benavent et al., 2014). However, to include the mineralogy of garnierites in greater detail, more information is required about the reactivity of these phases.

The aim of this work is to shed light on the control of the mineralogy and chemistry of garnierite on their dissolution kinetics under acidic pH conditions. To pursue this goal, we selected garnierite samples with a serpentine-, talc- and sepiolite-dominated mineralogy, studied in detail by Villanova-de-Benavent et al. (2014, 2016, 2019), to perform a kinetic study using flow-through experiments at pH 3 and 5, and 25 °C.

2. Geological setting

The samples selected for this study were collected in various Ni-laterite deposits of the Falcondo mining district, central Dominican Republic. These deposits formed after chemical weathering of the partially serpentinised Loma Caribe peridotite body, which consists of clinopyroxene-rich harzburgite, lherzolite, and dunite (Marchesi et al., 2016). These mantle peridotites underwent serpentinization, in the sub-oceanic floor scenario at moderate temperatures, through interaction with seawater (Lewis et al., 2006). The emplacement of the Loma Caribe peridotite body to its current tectonic position started in the late Albian, and it has been exposed to weathering and erosion since the early Miocene (Lewis et al., 2006; and references therein).

The weathering profile in Falcondo, like other hydrous Mg silicate-type Ni-laterite deposits worldwide, can be divided into three main units (from the base to the top): the partially serpentinised ultramafic protolith; a thick, serpentine-rich saprolite horizon; and a thinner, Fe-oxyhydroxide-rich limonite horizon. These layers vary in thickness, and their limits may not be horizontal. Garnierite mineralisation

Table 1
List of the selected samples including their mineralogy, average structural formulae, talc fraction (Xtlc), $\sum$octa/$\sum$tetra (octahedral versus tetrahedral cations: (Mg + Ni)/Si), and Mg/Si, Ni/Si and Ni/Mg ratios.

| label (Fig. 1)	sample (Fig. 1)	description	XRD	structural formula	number of analyses averaged	Xtlc (Fig. 2)	$\sum$octa/$\sum$tetra	Mg/Si	Ni/Si	Ni/Mg
Srp1/Xtlc$_{0.3}$Ni$_{0.8}$	09GAR-2	serpentine + traces kerolite-pimelite	7.32 Å	$(Mg_{2.06}Ni_{0.77}Fe_{0.14})Si_{2.64}O_{6.68}(OH)_{3.33} \cdot nH_2O$	6	0.34	1.13	0.78	0.29	0.37
Srp2/Xtlc$_{0.5}$Ni$_{1.4}$	LC100-II	serpentine + minor kerolite-pimelite	7.30 Å + 10.20 Å	$(Mg_{1.57}Ni_{1.37}Fe_{0.06})(Si_{2.84}Al_{0.07})O_{7.27}(OH)_{3.09} \cdot nH_2O$	7	0.45	1.03	0.55	0.48	0.87
Mix/Xtlc$_{0.4}$Ni$_{2.4}$	GAR-2	serpentine + kerolite-pimelite	7.40 Å + 10.56 Å	$(Ni_{2.42}Mg_{0.56}Fe_{0.01})Si_{2.71}O_{6.81}(OH)_{3.28} \cdot nH_2O$	4	0.36	1.1	0.21	0.89	4.32
Tlc1/Xtlc$_{0.8}$Ni$_{1.8}$	GAR-6	pimelite	10.14 Å (±7.34 Å)	$(Ni_{1.83}Mg_{1.17}(Si_{3.54}Al_{0.01})O_{8.88}(OH)_{2.45} \cdot nH_2O$	5	0.78	0.85	0.33	0.52	1.56
Tlc2/Xtlc$_{0.8}$Ni$_{1.9}$	LC100-IV	pimelite	9.94 Å (±7.39 Å)	$(Ni_{1.90}Mg_{1.10})(Si_{3.52}Al_{0.01})O_{8.83}(OH)_{2.47} \cdot nH_2O$	4	0.77	0.85	0.31	0.54	1.73
Sep1/SepNi$_{0.3}$	FALC-4	Ni-sepiolite	12.07 Å	$(Mg_{3.51}Ni_{0.26}Fe_{0.06})(Si_{6.05}Al_{0.01})O_{15}(OH)_2 \cdot 6H_2O$ [16]	16	–	0.63	0.58	0.04	0.07
Sep2/SepNi$_{2.0}$	FALC-3	falcondoite	12.15 Å	$(Mg_{2.03}Ni_{1.95}Fe_{0.01})(Si_{5.95}Al_{0.06})O_{15}(OH)_2 \cdot 6H_2O$	4	–	0.66	0.34	0.33	0.96
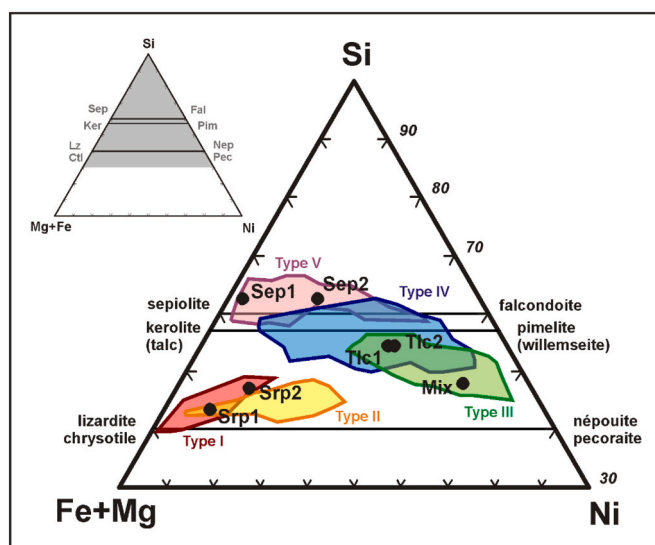
Fig. 1. Triangular plot showing the average composition (EMP) of the seven samples selected for the flow-through experiments (black circles), compared to the composition of the five garnierite types identified by Villanova-de-Benavent et al. (2014) (coloured fields), plotted as atoms per formula unit.
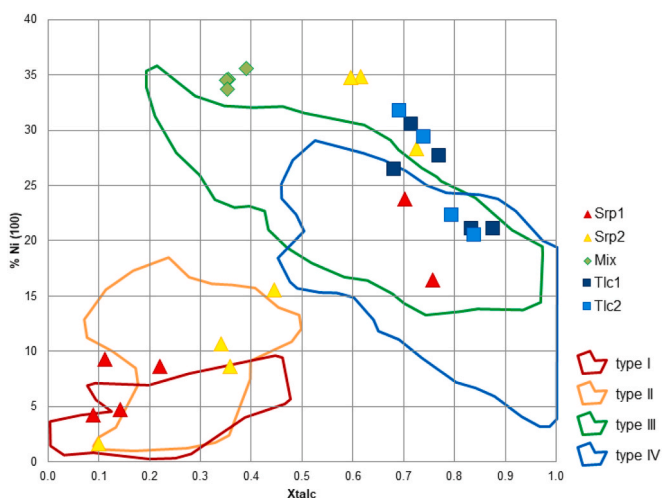

Fig. 2. Binary plot of the Ni content (calculated on the basis of 100 oxygens) versus the talc fraction (Xtlc) of representative analyses of the serpentine- and talc-like mixture samples selected for the dissolution experiments. The fields correspond to the Ni vs Xtlc of all the analysed samples by garnierite type (data from Villanova-de-Benavent et al., 2014).

commonly occurs as vein infillings, breccia cements, and coatings, at the bottom of the saprolite horizon. However, they may also be found crosscutting the unweathered serpentinised peridotite, as well as in the upper saprolite horizon (Villanova-de-Benavent et al., 2014).

In Falcondo, garnierites display various shades of green, and five types have been identified, according to their mineralogy. Types I to IV consist of mixtures of serpentine and kerolite-pimelite at the nanometre scale and in various proportions, from serpentine-dominated type I to kerolite-dominated type IV. Besides, type V is sepiolite-falcondoite (Villanova-de-Benavent et al., 2014, 2016, 2019).

3. Materials and methods

3.1. Garnierite sample characterisation

In this study seven samples were selected to represent in terms of

mineralogy and chemical composition the garnierite suite of the Falcondo Ni-laterite deposits (Dominican Republic). These samples correspond to: i. serpentine-dominated (labelled Srp1, Srp2 and Mix), ii. talc-dominated mixtures of serpentine- and talc-like garnierites (Tlc1 and Tlc2), and iii. sepiolite-like garnierites (Sep1 and Sep2; see Table 1, Figs. 1 and 2). A few grams of the selected samples were carefully hand-picked and screened for mineral impurities under the binocular stereomicroscope.

The samples were ground using an agate mortar and pestle, and were sieved in order to obtain a particle size between 53 and 106 μm. The specific surface area ($m^2 \cdot s^{-1}$) was determined by the Brunauer-Emmett-Teller (BET) method (Brunauer et al., 1938) with a Micromeritics ASAP 2000 surface area analyser using 5-point N_2 absorption isotherms.

The mineralogical composition of the samples was determined by means of powder X-ray diffraction (XRD) and the atomic ratios by Electron Microprobe (EMP) analyses. The X-ray diffractograms were collected through a PANalytical X'Pert PRO MPD Alpha1 powder diffractometer in Bragg-Brentano θ/2θ geometry of 240 mm of radius, nickel filtered Cu Kα radiation (λ = 1.5418 Å), and 45 kV–40 mA. During analysis, sample was spun at 2 revolutions per second. A variable divergence slit kept a constant illuminated area (10 mm) and a mask was used to limit the length of the beam (12 mm). Axial divergence Soller slits of 0.04 radians were used. Samples were scanned from 3 to 80° 2θ with step size of 0.017° and measuring time of 50 s per step, using a X'Celerator detector (active length = 2.122°). X'Pert Highscore® was used to substract the background of the diffractograms, and to carry out the qualitative analysis by assignment of the detected peaks to the corresponding d_{hkl} of mineral phases.

Hand-picked fragments from each sample were selected for EMP analysis. Point analyses were performed with a Cameca Electron Microprobe Analyser SX-50 equipped with four wavelength dispersive spectrometers (WDS) and an energy dispersive spectrometer (EDS). Analysis conditions were 20 kV, 15 nA, 2 μm beam diameter, counting time of 20 s per element and a take-off angle of 40°. The software used during data acquisition was XMAS (SAMx, France), which avail the matrix effect correction model PAP (Pouchou and Pichoir, 1991). The following calibration standards were used: hematite (Fe, LIF, Kα), rutile (Ti, PET, Kα), periclase (Mg, TAP, Kα), rhodonite (Mn, LIF, Kα), Al_2O_3 (Al, TAP, Kα), Cr_2O_3 (Cr, PET, Kα), metallic vanadium (V, LIF, Kα), diopside (Si, TAP, Kα), sphalerite (Zn, LIF, Kα), NiO (Ni, LIF, Kα) and wollastonite (Ca, PET, Kα).

Moreover, the texture and chemistry of the selected samples were examined after the experiments under a Field Emission Scanning Electron Microscope (FESEM) Jeol JSM-7100 at 20 kV. No precipitates were observed on the rugose surfaces of the samples after the experiments (Fig. 3).

3.2. Structural formulae

The structural formulae of serpentine and talc-like garnierite mixtures were calculated using 7 or 11 oxygens, depending on the dominant phase. The final formula was recalculated by considering the proportion of the talc-like (or serpentine-like) phase in the mixture. This proportion can be calculated on the basis of the formulae proposed by i) Brindley and Hang (1973) and ii) Soler et al. (2008). The formulae by Brindley and Hang (1973) are:

$$X_1 = 2 - 1.5 \times \frac{SiO_2}{MgO} \quad [1]$$

$$X_2 = 1.5 \times \frac{SiO_2}{MgO} - 1 \quad [2]$$

where X_1 is the proportion of serpentine layers in 10 Å-type (talc-like) garnierites, X_2 is the proportion of talc layers in 7 Å-type (serpentine-like) garnierites and SiO_2/MgO is the mole ratio of the oxides, calculated
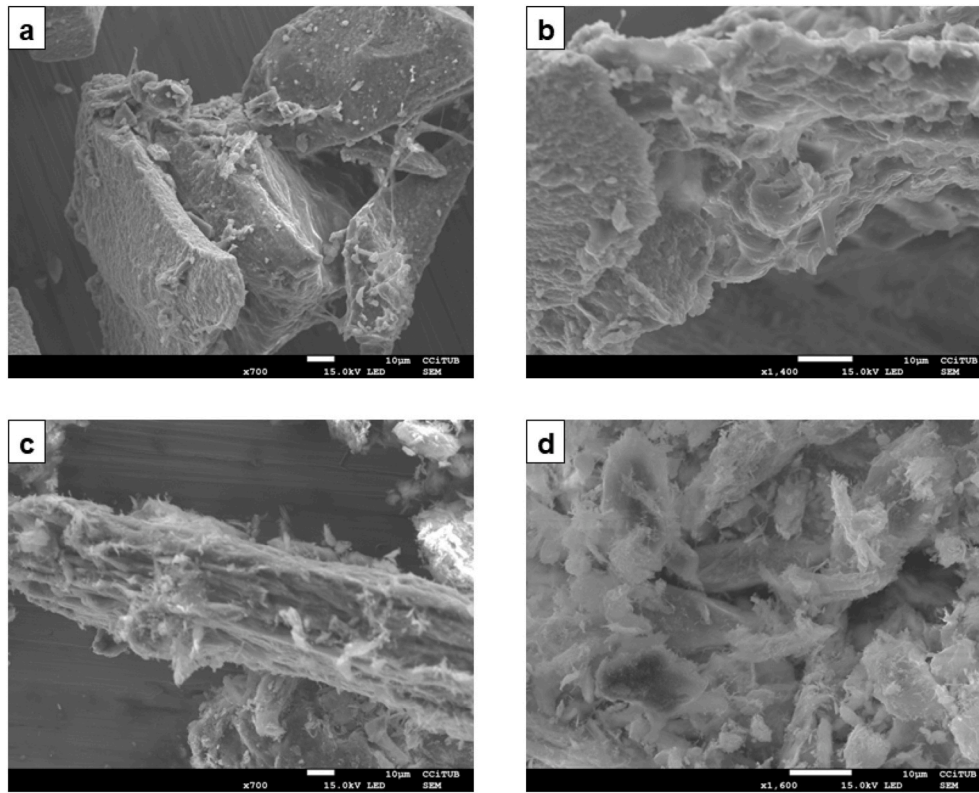
Fig. 3. Selected FESEM secondary electron photomicrographs of reacted samples: a-b) GAR-2 (Mix/$Xtlc_{0.4}Ni_{2.4}$) at pH 3 (a) and pH 5 (b); c-d) FALC-3 (Sep2/$SepNi_{2.0}$) at pH 3 (c) and pH 5 (d).

using the atoms per formula unit of these elements (here Mg includes Ni and other octahedral cations). Soler et al. (2008) proposed:

$$Xserp = \frac{1}{2} \times \left(4 - \frac{3}{\frac{Mg+Ni}{Si}} \right) \qquad [3]$$

$$Xtalc = 1 - Xserp \qquad [4]$$

where X_{serp} and X_{talc} are the respective serpentine and talc mole fractions in the garnierite mixture, and (Mg + Ni)/Si is the atomic ratio of these elements.

Both methods are based on the relationship between the cations in the octahedral and tetrahedral sites in serpentine and talc (equal to 3/2 and 3/4 respectively), and are equivalent (as X_1 in Eq. (1) and Xserp in Eq. (3) are the same). The formula used in this study for the calculation of the talc component in garnierites is as follows:

$$Xtlc = 1.5 \times \frac{\sum \text{tetra}}{\sum \text{octa}} - 1 \qquad [5]$$

where X_{tlc} is the talc component in garnierite mixtures (in mole fraction) and $\sum_{tetra}$ and $\sum_{octa}$ are the sum of the atoms per formula unit of cations occupying the tetrahedral (Si and Al) and octahedral (Mg, Ni and Fe) sites, respectively. In this study, the compositions of the serpentine- and talc-like mixture samples will also be indicated as $Xtlc_{0.3}Ni_{0.8}$, $Xtlc_{0.5}Ni_{1.4}$, $Xtlc_{0.4}Ni_{2.4}$, $Xtlc_{0.8}Ni_{1.8}$ and $Xtlc_{0.8}Ni_{1.9}$ (Table 1).

Mineral formulae for the sepiolite-falcondoite series were normalised to 32 oxygens. Sepiolite-like garnierite samples are referred to as $SepNi_{0.3}$ and $SepNi_{2.0}$ (Table 1). All Fe was considered to be Fe^{3+} in both the saprolite serpentine and the Fe-bearing garnierites, in accordance with Brindley and Hang (1973), Golightly and Arancibia (1979), Wells et al. (2009), and Roqué-Rosell et al. (2017). The tetrahedral layer was fully occupied by Si in most cases (as reported by Golightly and

Table 2
Dissolution reactions for the seven studied garnierite samples.

label	sample	reaction
Srp1	09GAR-2	$(Mg_{2.06}Ni_{0.77}Fe_{0.14})(Si_{2.64})O_{6.68}(OH)_{3.33} \cdot nH_2O +$ $6.08H^+ + 0.57H_2O$
$Xtlc_{0.3}Ni_{0.8}$		$= 2.06Mg^{2+} + 0.77Ni^{2+} + 0.14Fe^{3+} + 2.64H_4SiO_4 +$ nH_2O
Srp2	LC100-II	$(Mg_{1.57}Ni_{1.37}Fe_{0.06})(Si_{2.84}Al_{0.07})O_{7.27}(OH)_{3.09} \cdot nH_2O$ $+ 6.27H^+ + 1.0H_2O$
$Xtlc_{0.5}Ni_{1.4}$		$= 1.57Mg^{2+} + 1.37Ni^{2+} + 0.06Fe^{3+} + 0.07Al^{3+} +$ $2.84H_4SiO_4 + nH_2O$
Mix	GAR-2	$(Ni_{2.42}Mg_{0.56}Fe_{0.01})(Si_{2.71})O_{6.81}(OH)_{3.28} \cdot nH_2O +$ $5.99H^+ + 0.77H_2O$
Mix/ $Xtlc_{0.4}Ni_{2.4}$		$= 2.42Ni^{2+} + 0.56Mg^{2+} + 0.01Fe^{3+} + 2.71H_4SiO_4 +$ nH_2O
Tlc1	GAR-6	$(Ni_{1.83}Mg_{1.17})(Si_{3.54}Al_{0.01})O_{8.88}(OH)_{2.45} \cdot nH_2O +$ $6.03H^+ + 2.82H_2O$
$Xtlc_{0.8}Ni_{1.8}$		$= 1.83Ni^{2+} + 1.17Mg^{2+} + 0.01Al3+ + 3.54H_4SiO_4 +$ nH_2O
Tlc2	LC100-IV	$(Ni_{1.90}Mg_{1.10})(Si_{3.52}Al_{0.01})O_{8.83}(OH)_{2.47} \cdot nH_2O +$ $6.03H^+ + 2.79H_2O$
$Xtlc_{0.8}Ni_{1.9}$		$= 1.90Ni^{2+} + 1.10Mg^{2+} + 0.01Al^{3+} + 3.52H_4SiO_4 +$ nH_2O
Sep1	FALC-4	$(Mg_{3.51}Ni_{0.26}Fe_{0.06})(Si_{6.05}Al_{0.01})O_{15}(OH)_2 \cdot 6H_2O +$ $7.75H^+ + 1.21H_2O$
$SepNi_{0.3}$		$= 3.51Mg^{2+} + 0.26Ni^{2+} + 0.06Fe^{3+} + 0.01Al^{3+} +$ $6.05H_4SiO_4$
Sep2	FALC-3	$(Mg_{2.03}Ni_{1.95}Fe_{0.01})(Si_{5.95}Al_{0.06})O_{15}(OH)_2 \cdot 6H_2O +$ $8.17H^+ + 0.82H_2O$
Sep2/ $SepNi_{2.0}$		$= 2.03Mg^{2+} + 1.95Ni^{2+} + 0.01Fe^{3+} + 0.06Al^{3+} +$ $5.95H_4SiO_4$

Arancibia, 1979). According to the structural formula of the samples, the dissolution reactions of the studied garnierites from the Falcondo Ni-laterite deposit are expressed in Table 2.

Table 3

Experimental conditions and steady-state values used to calculate the dissolution rate constants (mol·m^{-2}·s^{-1}).

label (Fig. 1)	sample (Fig. 1)	duration (h)	initial pH	final pH	output Mg (µM)	output Ni	output Si	Mg/Si	(Mg + Ni)/Si	Ni/Si	Ni/Mg	initial mass (g)	initial BET surface (m²·g⁻¹)	final mass	final BET surface
Srp1	09GAR-2	3068	3.02	3.05	47.01	4.00	41.77	1.13	1.22	0.10	0.09	0.2170	106.4	0.1100	143.6
Xtlc$_{0.3}$Ni$_{0.8}$	09GAR-2	3068	4.61	6.12	10.24	1.80	10.81	0.95	1.11	0.17	0.18	0.1891	106.4	0.1781	110.0
Srp2	LC100-II	2299	2.997	3.03	23.38	3.90	24.74	0.95	1.10	0.16	0.17	0.1576	90.4	0.0409	116.6
Xtlc$_{0.5}$Ni$_{1.4}$	LC100-II	2299	4.66	5.75	14.73	1.77	14.19	1.04	1.16	0.12	0.12	0.1678	90.4	0.1552	109.8
Mix	GAR-2	1203	3.06	3.20	33.39	145.38	118.87	0.28	1.50	1.22	4.35	0.8342	103.4	0.7840	143.6
Xtlc$_{0.4}$Ni$_{2.4}$	GAR-2	1202	4.90	5.18	2.44	5.46	6.17	0.38	1.27	0.88	2.30	0.7863	103.4	0.7670	81.7
Tlc1	GAR-6	1527	3.02	3.05	15.73	15.13	11.35	1.39	2.72	1.33	0.96	0.3447	70.3	0.3119	125.8
Xtlc$_{0.8}$Ni$_{1.8}$	GAR-6	1528	4.90	5.30	2.83	3.06	5.18	0.55	1.14	0.59	1.08	0.3473	70.3	0.3406	125.5
Tlc2	LC100-IV	1100	3.03	3.05	10.09	11.67	19.37	0.52	1.12	0.60	1.16	0.4726	32.9	0.4424	106.7
Xtlc$_{0.8}$Ni$_{1.9}$	LC100-IV	1100	4.84	5.40	8.70	1.44	9.19	0.95	1.10	0.16	0.17	0.4805	32.9	0.4677	92.9
Sep1	FALC-4	998	3.04	3.14	40.95	3.28	35.01	1.17	1.26	0.09	0.08	0.1085	135.0	0.1004	183.4
SepNi$_{0.3}$	FALC-4	998	4.79	5.34	13.33	1.38	19.15	0.70	0.77	0.07	0.10	0.1122	135.0	0.1076	193.7
Sep2	FALC-3	998	3.07	3.18	67.04	16.78	84.99	0.79	0.99	0.20	0.25	0.3681	176.2	0.3400	181.2
SepNi$_{2.0}$	FALC-3	998	4.71	5.44	12.76	1.39	17.55	0.73	0.81	0.08	0.11	0.3409	176.2	0.3363	163.6

| label (Fig. 1)	sample (Fig. 1)	final pH	R$_{Mg\text{-}BET}$ (mol·m^{-2}·s^{-1})	R$_{Si\text{-}BET}$ (mol·m^{-2}·s^{-1})	R$_{Ni\text{-}BET}$ (mol·g^{-1}·s^{-1})	logR$_{Mg\text{-}BET}$ (mol·g^{-1}·s^{-1})	logR$_{Si\text{-}BET}$	logR$_{Ni\text{-}BET}$	R$_{Mg\text{-}mass}$	R$_{Si\text{-}mass}$	R$_{Ni\text{-}mass}$	logR$_{Mg\text{-}mass}$	logR$_{Si\text{-}mass}$	logR$_{Ni\text{-}mass}$
Srp1	09GAR-2	3.05	1.18E-12	5.39E-13	1.51E-13	−11.9	−12.3	−12.8	1.69E-10	7.76E-11	2.18E-11	−9.8	−10.1	−10.7
Xtlc$_{0.3}$Ni$_{0.8}$	09GAR-2	6.12	1.42E-13	1.15E-13	6.49E-14	−12.8	−12.9	−13.2	1.56E-11	1.26E-11	7.14E-12	−10.8	−10.9	−11.1
Srp2	LC100-II	3.03	3.07E-12	3.92E-13	9.11E-14	−11.5	−12.4	−13.0	4.12E-11	6.94E-11	1.61E-11	−10.4	−10.2	−10.8
Xtlc$_{0.5}$Ni$_{1.4}$	LC100-II	5.75	3.54E-13	1.82E-13	4.55E-14	−12.5	−12.7	−13.3	3.89E-11	2.00E-11	5.01E-12	−10.4	−10.7	−11.3
Mix	GAR-2	3.20	3.34E-13	2.45E-13	3.42E-13	−12.5	−12.6	−12.5	4.80E-11	3.52E-11	4.91E-11	−10.3	−10.5	−10.3
Xtlc$_{0.4}$Ni$_{2.4}$	GAR-2	5.18	6.92E-14	3.55E-14	3.53E-14	−13.2	−13.4	−13.5	5.67E-12	2.91E-12	2.90E-12	−11.2	−11.5	−11.5
Tlc1	GAR-6	3.05	2.72E-13	5.96E-14	1.57E-13	−12.6	−13.2	−12.8	3.43E-11	7.49E-12	1.98E-11	−10.5	−11.1	−10.7
Xtlc$_{0.8}$Ni$_{1.8}$	GAR-6	5.30	4.45E-14	2.59E-14	3.02E-14	−13.4	−13.6	−13.5	5.59E-12	3.25E-12	3.79E-12	−11.3	−11.5	−11.4
Tlc2	LC100-IV	3.05	1.58E-13	9.12E-14	1.02E-13	−12.8	−13.0	−13.0	1.69E-11	9.73E-12	1.09E-11	−10.8	−11.0	−11.0
Xtlc$_{0.8}$Ni$_{1.9}$	LC100-IV	5.40	1.40E-13	4.53E-14	1.30E-14	−12.9	−13.3	−13.9	1.30E-11	4.20E-12	1.21E-12	−10.9	−11.4	−11.9
Sep1	FALC-4	3.14	4.83E-13	2.29E-13	5.45E-13	−12.3	−12.6	−12.3	8.85E-11	9.99E-11	4.20E-11	−10.1	−10.0	−10.4
SepNi$_{0.3}$	FALC-4	5.34	1.42E-13	1.18E-13	1.97E-13	−12.8	−12.9	−12.7	2.75E-11	2.28E-11	3.82E-11	−10.6	−10.6	−10.4
Sep2	FALC-3	3.18	4.29E-13	1.75E-13	1.08E-13	−12.4	−12.8	−13.0	7.78E-11	3.18E-11	1.96E-11	−10.1	−10.5	−10.7
SepNi$_{2.0}$	FALC-3	5.44	9.17E-14	4.28E-14	1.03E-14	−13.0	−13.4	−14.0	1.50E-11	7.00E-12	1.69E-12	−10.8	−11.2	−11.8
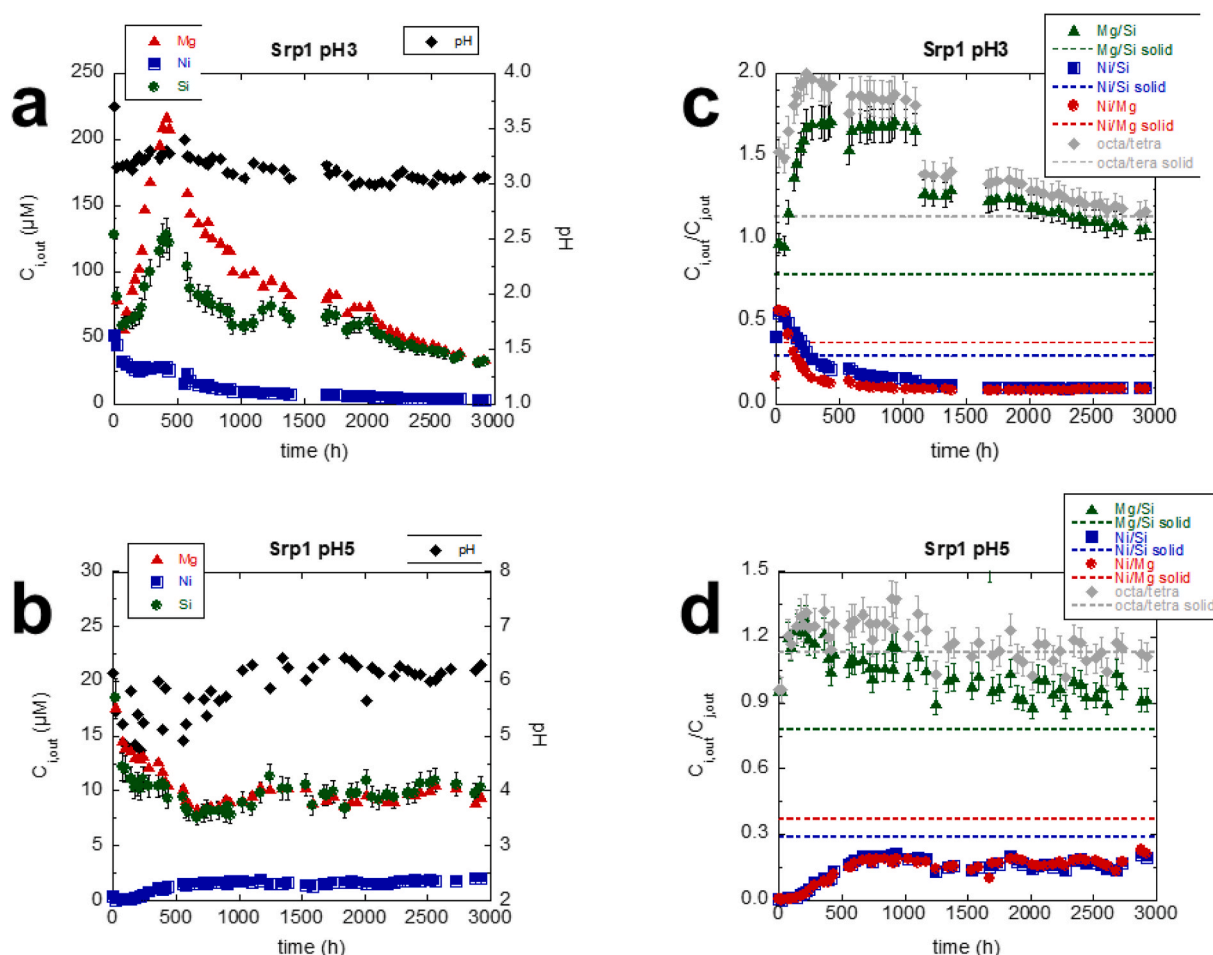
Fig. 4. Variation in the output concentrations of Mg, Ni and Si (a,b) and Mg/Si, Ni/Si, Ni/Mg and octahedral/tetrahedral ratios (c,d) as a function of time for sample Srp1 (Xtlc$_{0.3}$Ni$_{0.8}$) at input pH of 3 and 5. Dashed lines showed the stoichiometric ratios of the solids (see Table 1).

3.3. Experimental setup

In the experiments, a known mass of garnierite was placed in a re-action cell (ca. 35 mL in volume), with a continuous flow of a solution with pH of 3 or 5, until steady state was achieved (from 1000 up to 3000 h). According to the procedure described by Metz and Ganor (2001), non-stirred flow-through experiments were carried out by using reaction cells composed of two chambers; a lower chamber with an inner diameter of 33 mm and an upper chamber with an inner diameter of 26 mm. The two chambers were separated by a 5 μm nylon mesh, on which the sample powder was placed (see details in Cama and Acero, 2005). For each sample two experiments were carried out, one with an input solution of pH 3 and the other 1 at pH = 5 (Table 3). The cells were connected with the input solutions by a tube (inner diameter 38 μm) through a Gilson peristaltic pump that controlled an input flow rate of 0.04 mL min^{-1}, which was held constant over the experimental dura-tion, yielding a mean water residence time of ≈15 h. The output solution was collected in a closed polytetrafluoroethylene (PTFE) plastic bottle, and was sampled periodically for analysis. Steady state was achieved when the output Mg, Ni and Si concentrations remained approximately constant and differed by less than 5% between consecutive samples (at least 500 h).

The steady-state dissolution rate R (mol m^{-2} s^{-1}) was calculated from the release of Si, Mg and Ni according to the expression (Nagy et al., 1991):

$$R = \frac{q}{v_j A}\left(C_{j,\ out} - C_{j,\ inp}\right) \qquad [6]$$

where v_j is the stoichiometric coefficient of component j in the disso-lution reaction, q is the flow rate (m^3 s^{-1}), A is the reactive surface area (m^2) calculated with the final mass (g) and the final BET surface area (m^2 g^{-1}), and $C_{j,inp}$ and $C_{j,out}$ are the concentrations of component j (Si, Mg, Ni) in the input and the output solutions, respectively (mol m^{-3}) (Table 3). $C_{j,inp}$ (Si, Mg, Ni) was always zero. The propagated error associated with the calculated dissolution rate was estimated to be approximately 15%, according to the Gaussian error propagation method (Cama and Acero, 2005).

After the conclusion of the experiments, the cells were dismantled, and the powder samples were retrieved, vacuum-dried, weighted and stored until their BET surface area was measured. In most cases, the final BET surface areas were higher (82–194 m^2 g^{-1}) than the initial ones (33–176 m^2 g^{-1}, Table 3).

The measured $C_{Mg,out}$, $C_{Ni,out}$, $C_{Fe,out}$, $C_{Al,out}$ and $C_{Si,out}$, the $\Sigma_{oct}/\Sigma_{tetra}$ ratio, (defined as the ratio between $C_{j,out}$ of the octahedral and tetra-hedral cations [$C_{Mg,out} + C_{Ni,out} + C_{Fe,out}$]/[$C_{Si,out} + C_{Al,out}$]), and the Mg/Si and Ni/Si ratios have been used to evaluate the relationship be-tween the release of octahedral and tetrahedral cations. Additionally, the Ni/Mg ratio has been used to evaluate the behaviour of these octa-hedral cations. These ratios are suitable to monitor changes in the re-action stoichiometry over the experiments.

3.4. Solution analyses

Input solutions were prepared with Millipore MQ water (18.2 MΩ cm at 25 °C) and reagent grade HCl (Merck). The pH of the input and output
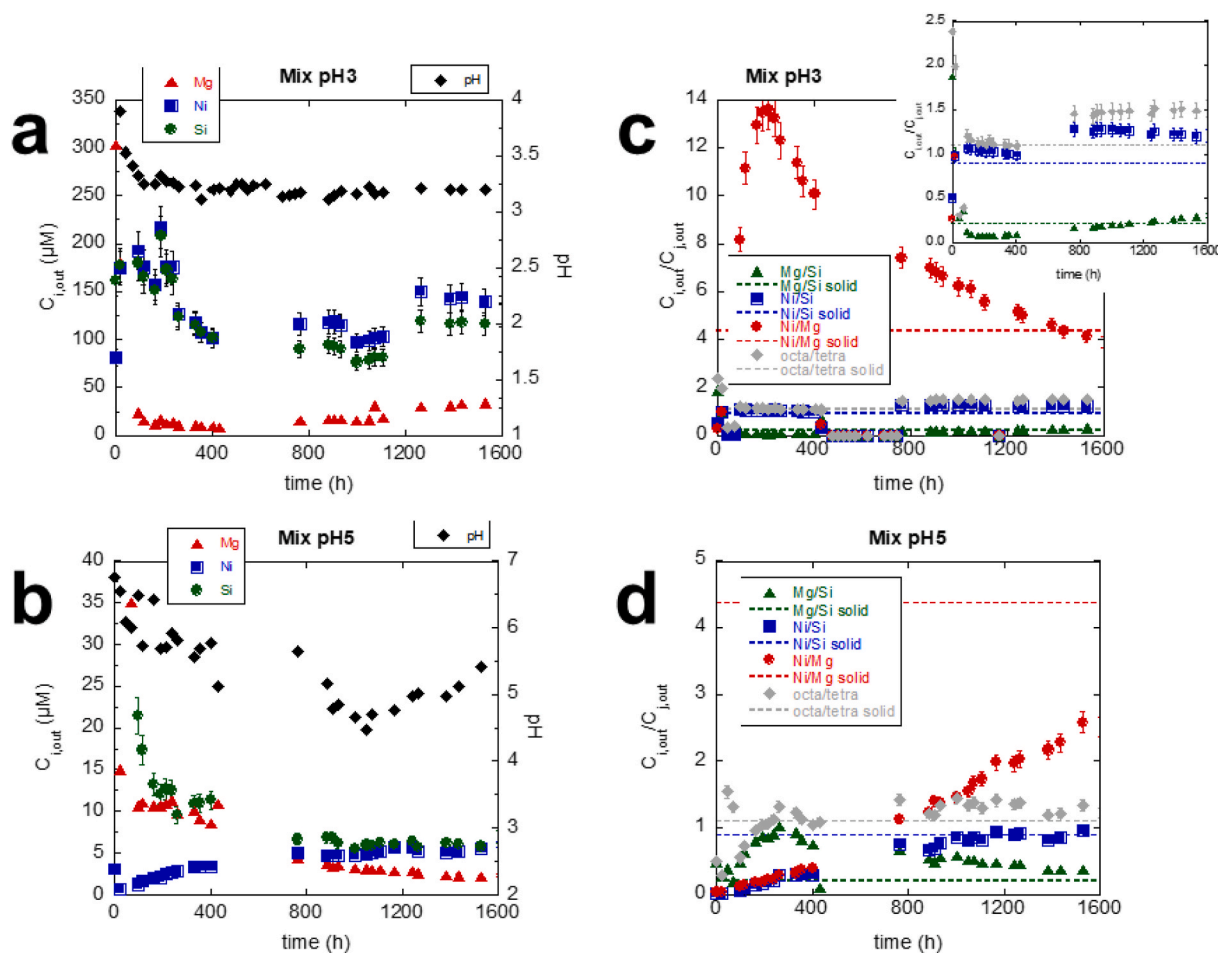
Fig. 5. Variation in the output concentrations of Mg, Ni and Si (a,b) and Mg/Si, Ni/Si, Ni/Mg and octahedral/tetrahedral ratios (c,d) as a function of time for sample Mix (Xtalc$_{0.4}$Ni$_{2.4}$) at input pH of 3 and 5. Dashed lines showed the stoichiometric ratios of the solids (see Table 1).

solutions was measured with a ThermoScientific Orion© combined glass electrode at room temperature (~25 °C). The uncertainty was ±0.02 pH units.

Output concentrations of Si, Ni, Mg, Fe and Al were measured by Inductively Coupled Plasma-Optical Emission Spectrometry (ICP-OES), using a Thermo Jarrel-Ash spectrometer equipped with a CID detector at the IDAEA-CSIC. The accuracy of ICP-OES measurement was estimated to be around 3%. The detection limits for Si, Ni, Mg, Fe and Al were 7×10^{-7}, 9×10^{-8}, 2×10^{-6}, 2×10^{-7} and 8×10^{-7} mol L^{-1}, respectively.

3.5. Solution saturation state

The degree of saturation of the output solutions with respect to Si-, Mg-, and Ni-bearing phases was calculated using the PHREEQC code, version 2.15.0 (Parkhurst and Appelo, 1999) and with the LLNL thermodynamic database. Calculations showed that during the experiments the output solutions were highly undersaturated with respect to Si, Mg and Ni bearing phases (e.g. Mg(OH)$_2$, Ni(OH)$_2$, chrysotile, sepiolite, talc, anthophyllite, antigorite, enstatite, forsterite, Ni$_2$SiO$_4$) and slightly undersaturated with respect to quartz.

4. Results

The results of all the experiments are presented in Table 3, and Figs. 4–7 show the time evolution of Mg, Ni and Si concentrations in absolute values for selected experiments, which are representative to serpentine-, talc- and sepiolite-dominated garnierites. They also show the time evolution of the ratios Mg/Si, Ni/Si, Ni/Mg and octahedral/

tetrahedral cations compared to theoretical stoichiometric ratios (dashed lines), in order to see whether the dissolution is stoichiometric or not. The experimental results show that: i. Mg, Ni and Si output concentrations throughout the experiments were higher at pH = 3 (mostly between 10 and 200 μM) than at pH = 5 (being below 20 μM) (Figs. 4–7); ii. when the pH in the input solution was 3, the output pH remained mostly unchanged, and when the input pH was 5, the output pH experienced only a slight variation (pH between 5 and 6, Figs. 4–7).

4.1. Serpentine-dominated garnierites

The variation of output concentrations of Mg, Ni and Si and pH as a function of time in the experiment with sample Srp1 (Xtalc$_{0.3}$Ni$_{0.8}$) is shown in Fig. 4. At pH = 3 (Fig. 4a), $C_{Mg,out} > C_{Si,out}$ in most of the experimental run and both decrease with time. $C_{Ni,out}$ also decreased with time at pH 3 (Fig. 4a). At pH = 5 (Fig. 4b), $C_{Mg,out} \approx C_{Si,out}$ in most of the experimental run. At this pH, $C_{Ni,out}$ starts increasing and reaches steady state at the same time as $C_{Mg,out}$ and $C_{Si,out}$.

Regarding stoichiometry, Mg is released in excess over Si at both pH values (Fig. 4c and d). During the early stages of the experiments, the Mg/Si ratio rapidly increases and with time it reduces and tends to the stoichiometric values, (stoichiometry is only approximated at pH = 5). The octa/tetra ratio tends to stoichiometry at both pH 3 and 5. At pH 3, the Ni/Mg and Ni/Si ratios start close to the stoichiometric values, but a Ni deficit occurs with time with both ratios well below the ones of the solid. The trends of $C_{i,out}$ and stoichiometric ratios in experiment Srp2 at pH of 3 and 5 are similar to those for experiment Srp1.

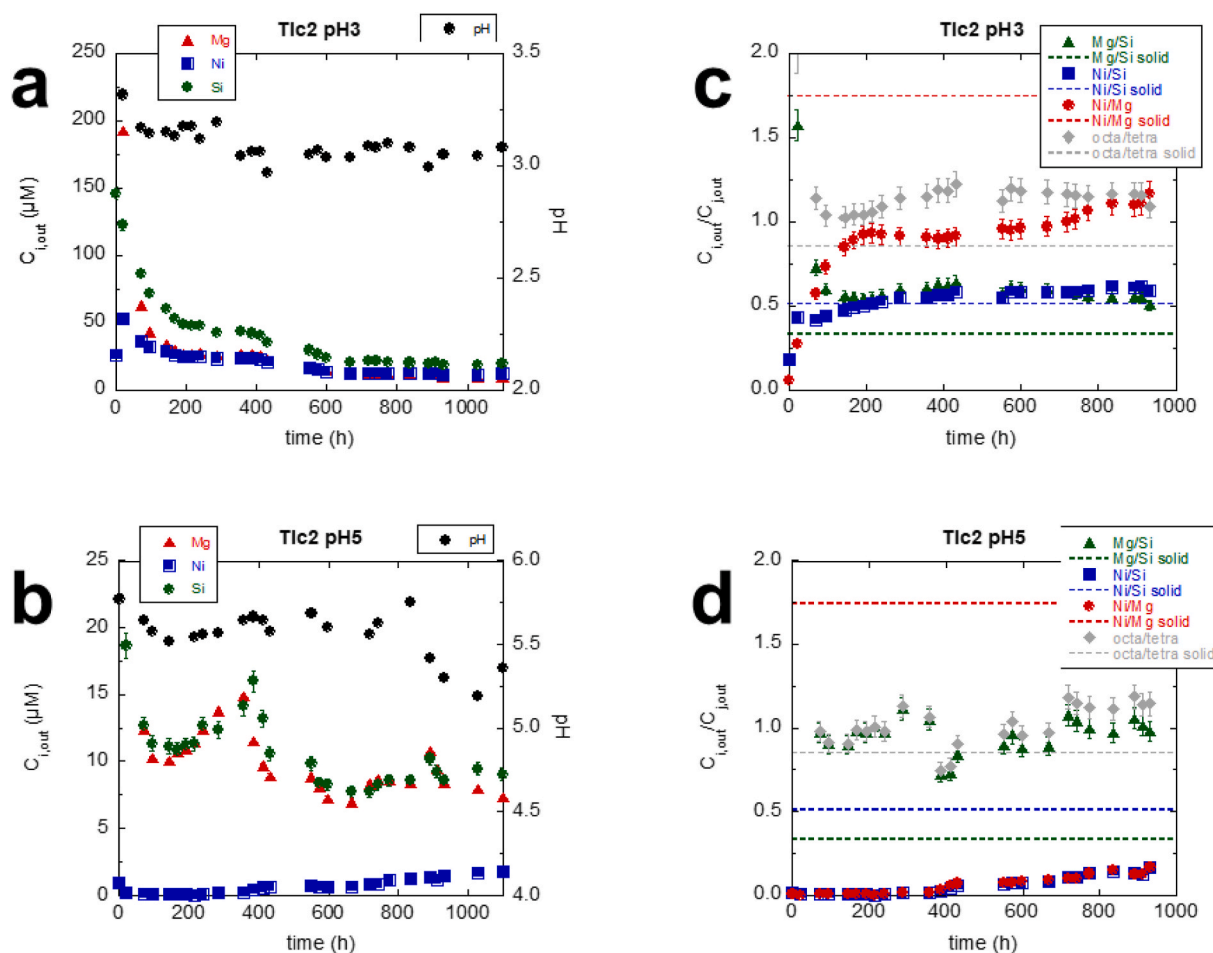The results show that the release of Mg in both Srp1 and Srp2 is

Fig. 6. Variation in the output concentrations of Mg, Ni and Si (a,b) and Mg/Si, Ni/Si, Ni/Mg and octahedral/tetrahedral ratios (c,d) as a function of time for sample Tlc2 ($Xtalc_{0.8}Ni_{1.9}$) at input pH of 3 and 5. Dashed lines showed the stoichiometric ratios of the solids (see Table 1).

consistently faster than those of Si (tetrahedral cation) and Ni (octahedral cation). Therefore, the release of Mg at steady state is used to calculate the dissolution rate (R_{diss}), which is higher at pH $\approx$ 3 ($logR_{Mg=}-11.9$ and -11.5 mol m^{-2} s^{-1}) than at pH $\approx$ 5 ($logR_{Mg} = -12.8$ and -12.5 mol m^{-2} s^{-1}) (Table 3).

The variation of output concentrations of Mg, Ni and Si and pH as a function of time in the experiment with sample Mix ($Xtlc_{0.4}Ni_{2.4}$) is shown in Fig. 5. At pH of 3 and 5, $C_{i,out}$ tends to increase rapidly to reach a maximum, and thereafter decreases and reaches steady state (Fig. 5a and b).

The Mg/Si ratio tends to stoichiometry at pH = 3, while at pH = 5, it reaches a maximum, decreases and also tends to stoichiometry (Fig. 5c and d). At pH = 3 the Ni/Mg ratio shows a maximum well above the stoichiometric ratio and thereafter decreases to stoichiometry. At pH = 5, it increases and tends gradually towards stoichiometry. The Ni/Si ratio is above stoichiometry all over the experiment at pH 3 and approaches stoichiometry at pH = 5.

4.2. Talc-dominated garnierites

The variation of output concentrations of Mg, Ni and Si and pH as a function of time in the experiment with sample Tlc2 ($Xtlc_{0.8}Ni_{1.9}$) is shown in Fig. 6a and b. $C_{Si,out}$ and $C_{Mg,out}$ show an early rise and then decrease and reach steady state at both pH values. $C_{Ni,out}$ behaves similarly at pH 3 but it increases gradually at pH 5. Output concentrations in experiment Tlc1 were more irregular and slightly different from those of experiment Tlc2 (Table 3).

The Mg/Si and octa/tetra ratios are above the values in the solids,

indicating Si deficit. At pH~5 the octa/tetra is close to the solid ratio. The Ni/Mg ratio is well below the solid one at both pH values (Fig. 6c and d). The Ni/Si ratio is slightly higher than in the solid at pH 3 and smaller than in the solid at pH = 5.

The dissolution rates at steady state are calculated based on the release of Mg, which in this case is similar at both pH values ($logR_{Mg=}-12.8$ mol m^{-2} s^{-1} at pH = 3.1 and -12.9 mol m^{-2} s^{-1} at pH = 5.4; Table 3).

4.3. Sepiolite-falcondoite

The variation of output concentrations of Mg, Ni and Si and pH as a function of time in the experiment with sample Sep2 (falcondoite, Ni-dominated sepiolite ($SepNi_{2.0}$)) is shown in Fig. 7a and b. During the early stages of the experiment, $C_{Si,out}$ and $C_{Mg,out}$ rise up to thereafter decrease. Steady state is obtained at both pH values. $C_{Ni,out}$ starts increasing, reaches a maximum, decreases thereafter and reaches steady state.

At both input pH values, an early rapid increase in the Mg/Si and oct/tetra ratios is observed before stabilization at high values is reached. At pH $\approx$ 5 the oct/tetra ratio is closer to the solid ratio (Fig. 7c and d). The high Mg/Si and oct/tetra ratios indicate strong Si deficit. Also, a Ni deficit is deduced at both pH values from the low Ni/Si and the Ni/Mg ratios.

The Mg-based dissolution rates of the sepiolite samples (Sep1 and Sep2) at steady state are faster at pH = 3 ($logR_{Mg} = -12.3$ and -12.4 mol m^{-2} s^{-1}) than at pH = 5 ($logR_{Mg} = -12.8$ and -13.0 mol m^{-2} s^{-1}; Table 3).
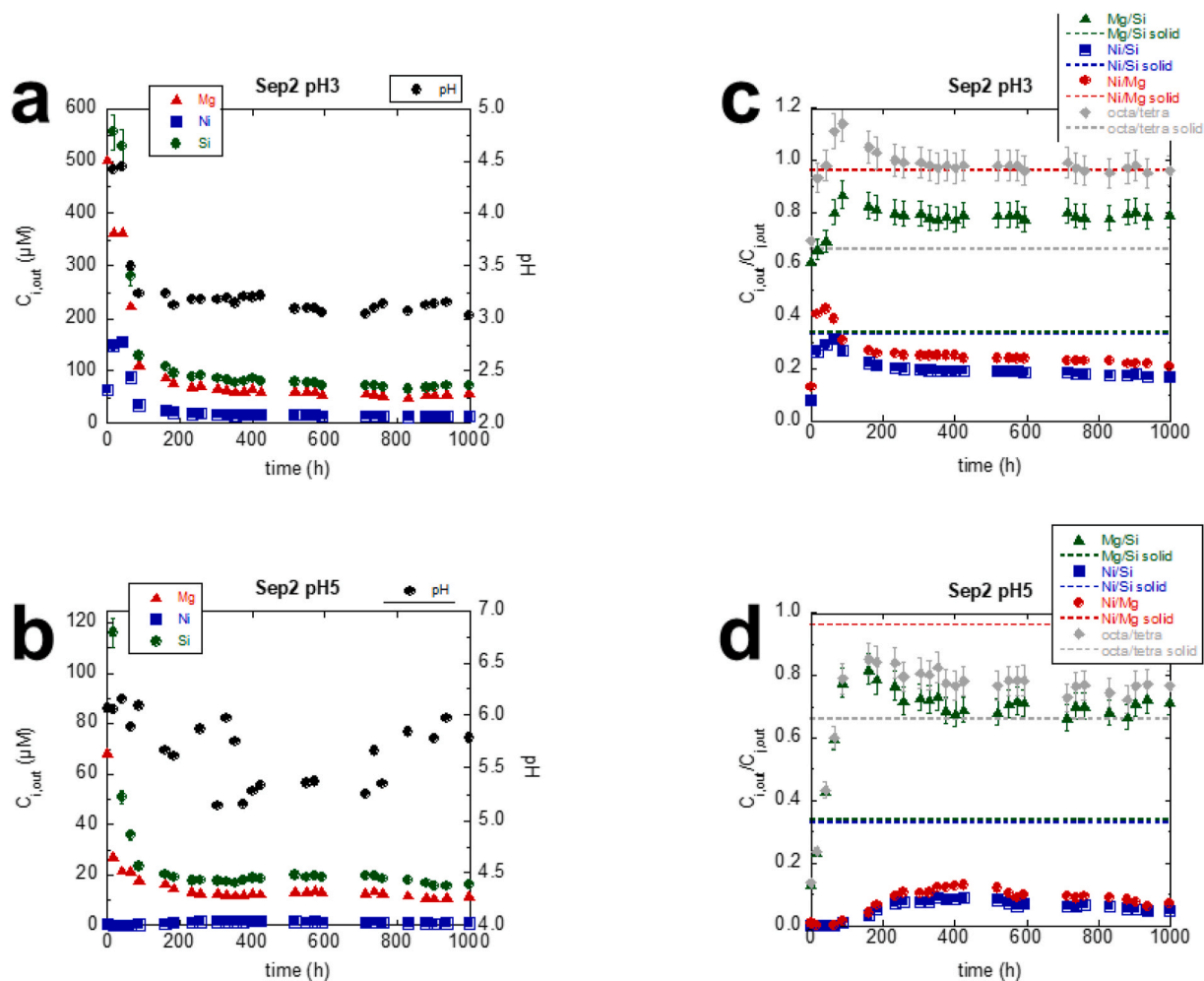
Fig. 7. Variation in the output concentrations of Mg, Ni and Si (a,b) and Mg/Si, Ni/Si, Ni/Mg and octahedral/tetrahedral ratios (c,d) as a function of time for sample Sep2 (SepNi$_{2.0}$) at input pH of 3 and 5. Dashed lines showed the stoichiometric ratios of the solids (see Table 1).
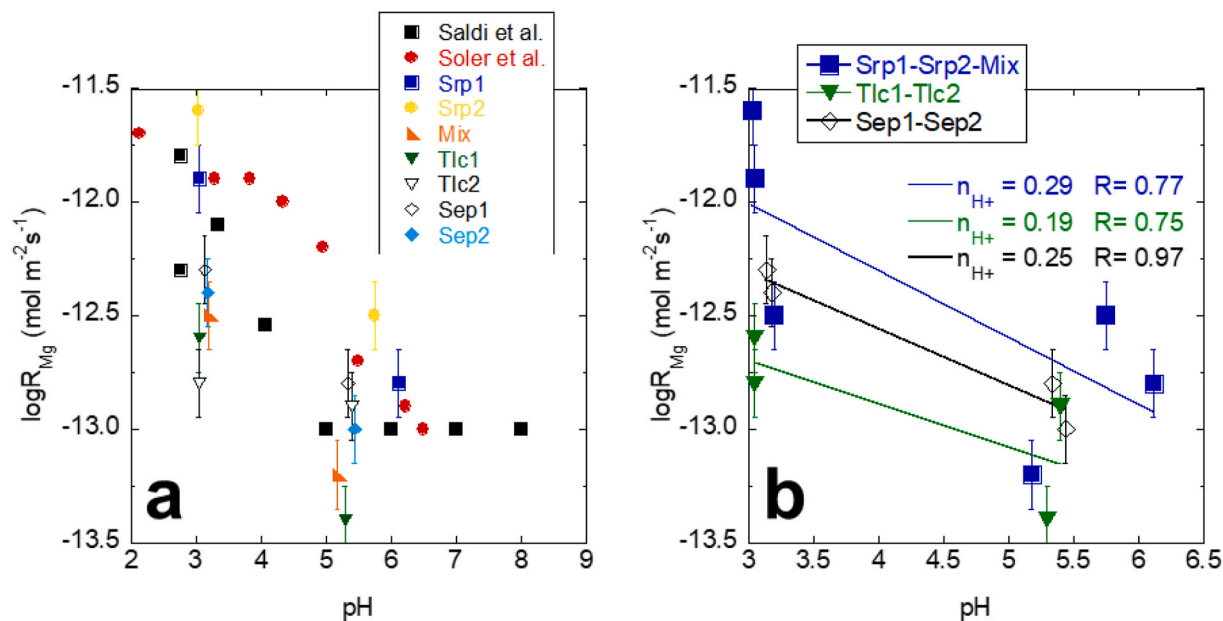

Fig. 8. Variation of the dissolution rate as a function of pH: a) dissolution rates obtained in this study and those of talc (Saldi et al., 2007) and garnierite (Soler et al., 2008); b) Linear regressions for dissolution rates of serpentine (Srp1 and Srp2), talc (Tlc1 and Tlc2) and sepiolite (Sep1 and Sep2) versus pH to obtain the values of k_{H+} and n_{H+} according to eq. (7).

5. Discussion

5.1. Stoichiometry of the reaction

The observed fluctuation of the Mg/Si and octa/tetra ratios indicate that Mg release is faster than that of Si, which is consistent with the garnierite behaviour described for the Loma de Hierro deposit (Soler et al., 2008). The slighter variations of the Ni/Si and Ni/Mg ratios indicate a systematic Ni deficit with the exception of the Mix sample ($Xtlc_{0.4}Ni_{2.4}$) at pH~3, where Ni/Mg is initially higher than the ideal one (Fig. 5c).

Preferential release of Mg over Si has been documented in several studies. Soler et al. (2008) observed that the dissolution is congruent at pH > 5 and incongruent at pH < 5, indicating a different contribution from serpentine and talc to the total dissolution process, because the serpentine component of the garnierite mixture dissolves faster under more acidic conditions. The faster dissolution of serpentine would cause the preferential release of Mg. Furthermore, Stoessell (1988) and Jones (1986), observed a more profound metastability of kerolite relative to sepiolite at 25 °C and 1 atm over a time span of 10 years.

Also, the rapid release of Mg with respect to Si detected in this study was already observed by Luce et al. (1972), who tested the dissolution of serpentine at pH between 1.6 and 9 and at 25 °C, and by Hume and Rimstidt (1992) when dissolving chrysotile at pH between 2 and 6 at 37 °C. The authors explained that the initial Mg release was due to a stoichiometric exchange of one Mg^{2+} for two H^+ from the aqueous solution. Lin and Clemency (1981) observed that Mg from the octahedral sheets was released more rapidly than Si from the tetrahedral sheets, when dissolving talc at pH close to 5 and at 25 °C in a closed system reactor. They suggested that talc dissolution rates are controlled by the destruction of the slower tetrahedral Si–O bonds.

In agreement with Luce et al. (1972), Lin and Clemency (1981) and Jurinski and Rimstidt (2001), Saldi et al. (2007) explained that under acidic pH, Mg is initially preferentially removed from the talc surface but at basic pH it is preferentially retained in agreement with the relative fast equilibration of the Mg for proton exchange reaction. These observations were performed based on dissolution experiments of talc at pH between 1 and 10.6 and temperatures between 25 and 150 °C, and it should be noted that their experiments were supersaturated with respect to one or more secondary phases, and in one case with respect to talc itself.

5.2. Dissolution rate pH-dependence

Serpentine-dominated garnierites (Srp1, Srp2 and Mix; Figs. 4 and 5) are prone to a faster release of Mg, Ni and Si than talc-dominated garnierites (Tlc1 and Tlc2; Fig. 6) and sepiolite-falcondoite (Sep1 and Sep2; Table 3 and Figs. 7 and 8).

The dissolution rate pH-dependence is calculated according to the following equation:

$$R_{Mg} = k_{H^+} \times a_{H^+}^{n_{H^+}} \qquad [7]$$

where R_{Mg} is the Mg-based dissolution rate, k_{H^+} is the dissolution rate constant and $a_{H^+}^{n_{H^+}}$ is the dependence on the activity of H^+. Fig. 8a shows that the obtained R_{Mg} for the garnierite samples decrease by increasing pH. The derived values for k_{H+} and n_{H+} range from $10^{-11.3}$ to $10^{-12.2}$ mol m^{-2} s^{-1} and from 0.19 to 0.30, respectively (Fig. 8b): serpentine ($R_{Mg} = -10^{-11.3} \cdot a_H^{0.25}$), talc ($R_{Mg} = -10^{-12.1} \cdot a_H^{0.19}$) and sepiolite ($R_{Mg} = -10^{-11.6} \cdot a_H^{0.25}$). There is no correlation between n_{H^+} X_{tlc} and Ni/Si ratio.

Jurinski and Rimstidt (2001) observed little to no pH-rate dependence for talc dissolution at pH 2–8 and 37 °C in mixed-flow reactors, in contrast to Saldi et al. (2007) who showed that the talc dissolution rate decreases with pH at pH < 6. Soler et al. (2008) reported rate-pH dependence for from Loma de Hierro (Venezuela) with $n_{H+} = 0.28$.

The obtained rates are comparable to those reported by Soler et al. (2008) for the Loma de Hierro garnierite with little Ni content and by Saldi et al. (2007) for talc. It appears that the rates are about two orders of magnitude slower than those of chrysotile obtained at pH 7–10 and 25 °C in batch experiments (Bales and Morgan, 1985).

6. Summary and conclusions

The results show that the dissolution rates of the garnierites from the Falcondo deposit decrease by increasing pH. This is consistent with garnierite rates from Loma de Hierro, Venezuela (Soler et al., 2008). In addition, the dissolution rates of serpentine-dominated garnierites are faster than those of talc (kerolite)-dominated garnierites and sepiolite-falcondoite. In general, the behaviour of the studied garnierites from the Falcondo Ni-laterite is comparable to that of Ni-free serpentine, talc, kerolite and sepiolite from the literature, with release of Mg faster than that of Si. In particular, in the mixtures of serpentine and talc, the excess of octa/tetra and Mg/Si molar ratios in comparison with the molar solid ratio may indicate that the phase that is being dissolved is the one with less silica, that is to say, serpentine (instead of talc). Therefore, the dissolution is not congruent.

It is widely observed that the system (Ni–Mg-phyllosilicates in contact with an acidic solution) preferentially retains Ni, and to a lesser extent Si (Ni and Si are the elements with the slowest release), which may favour the precipitation of Ni- and Si- rich phases in the profile.

The kinetic rate laws that have been derived from the experimental results can already be applied in the reactive transport modelling of the origin and evolution of these weathering profiles. In addition, another significant outcome is the occurrence of a non-stoichiometric dissolution at both pH ≈ 3 and pH ≈ 5–6. Further work would be needed for a more mechanistic interpretation of the results, by also integrating experiments under neutral or slightly alkaline conditions, and considering the use of solid solution models (incongruent dissolution).

Declaration of competing interest

The authors declare that they have no known competing financial interests or personal relationships that could have appeared to influence the work reported in this paper.

References

Bales, R.C., Morgan, J.J., 1985. Dissolution kinetics of chrysotile at pH 7 to 10. Geochem. Cosmochim. Acta 49, 2281–2288.

Brindley, G.W., Hang, P.T., 1973. The nature of garnierite: I. Structure, chemical compositions and color characteristics. Clay Clay Miner. 21, 27–40.

Brunauer, S., Emmet, P., Teller, E., 1938. Adsorption of gases in multimolecular layers. J. Am. Chem. Soc. 60, 309–319.

Butt, C.R.M., Cluzel, D., 2013. Nickel Laterite Ore Deposits: Weathered Serpentinites. Elements 9, 123–128.

Cama, J., Acero, P., 2005. Dissolution of minor sulphides present in a pyritic sludge at pH 3 and 25°C. Geol. Acta 3, 15–26.

Cathelineau, M., Quesnel, B., Gautier, P., Boulvais, P., Couteau, C., Drouillet, M., 2016. Nickel dispersion and enrichment at the bottom of the regolith: formation of pimelite target-like ores in rock block joints (Koniambo Ni deposit, New Caledonia). Miner. Deposita 51, 271–282.

Domènech, C., Galí, S., Villanova-de-Benavent, C., Soler, J.M., Proenza, J.A., 2017. Reactive transport model of the formation of oxide type Ni-laterite profiles (Punta Gorda, Moa Bay, Cuba). Miner. Deposita. https://doi.org/10.1007/s00126-017-0713-0.

Freyssinet, Ph, Butt, C.R.M., Morris, R.C., 2005. Ore-forming processes related to lateritic weathering. Econ. Geol. 100th Ann 681–722.

Fritsch, E., Juillot, F., Dublet, G., Fonteneau, L., Fandeur, D., Martin, E., Caner, L., Auzende, A.-L., Grauby, O., Beaufort, D., 2015. An alternative model for the formation of hydrous Mg/Ni layer silicates ('deweylite'/'garnierite') in faulted peridotites of New Caledonia: I. Texture and mineralogy of a paragenetic succession of silicate infillings. Eur. J. Mineral 28, 295–311.

Fu, W., Yang, J.W., Yang, M.L., Pang, B.C., Liu, X.J., Niu, H.J., Huang, X.R., 2014. Mineralogical and geochemical characteristics of a serpentinite-derived laterite profile from East Sulawesi, Indonesia: implications for the lateritization process and Ni supergene enrichment in the tropical rainforest. J. Asian Earth Sci. 93, 74–88.

Galí, S., Soler, J.M., Proenza, J.A., Lewis, J.F., Cama, J., Tauler, E., 2012. Ni-enrichment and stability of Al-free garnierite solid solutions: a thermodynamic approach. Clay Clay Miner. 60, 121–135.

Golightly, J.P., Arancibia, O.N., 1979. The chemical composition and infrared spectrum of nickel- and iron-substituted serpentine from a nickeliferous laterite profile, Soroako, Indonesia. Can. Mineral. 17, 719–728.

Hume, L.A., Rimstidt, J.D., 1992. The biodurability of chrysotile asbestos. Am. Mineral. 77, 1125–1128.

Jones, B.F., 1986. Clay mineral diagenesis in lacustrine sediments. In: Mumpton, F.A. (Ed.), Studies in diagenesis 1578, 291–300. USGS Bull.

Jurinski, J.B., Rimstidt, J.D., 2001. Biodurability of talc. Am. Mineral. 86, 392–399.

Lewis, J.F., Draper, G., Proenza, J.A., Espaillat, J., Jiménez, J., 2006. Ophiolite-Related Ultramafic Rocks (Serpentinites) in the Caribbean Region: A Review of their Occurrence, Composition, Origin, Emplacement and Ni-Laterite Soil Formation. Geol. Acta 4, 237–26.

Lin, F.-C., Clemency, C.V., 1981. The dissolution kinetics of brucite, antigorite, talc, and phlogopite at room temperature and pressure. Am. Mineral. 66, 801–806.

Luce, R.W., Bartlett, R.W., Parks, G.A., 1972. Dissolution kinetics of magnesium silicates. Geochem. Cosmochim. Acta 36, 35–50.

Marchesi, C., Garrido, C.J., Proenza, J.A., Hidas, K., Varas-Reus, M.I., Butjosa, L., Lewis, J.F., 2016. Geochemical record of subduction initiation in the sub-arc mantle: insights from the Loma Caribe peridotite (Dominican Republic). Lithos 252–253, 1–15.

Metz, V., Ganor, J., 2001. Stirring effect on kaolinite dissolution rate. Geochem. Cosmochim. Acta 20, 3475–3490.

Nagy, K.L., Blum, A.E., Lasaga, A.C., 1991. Dissolution and precipitation kinetics of kaolinite at 80 °C and pH 3. Am. J. Sci. 291, 649–686.

Parkhurst, D.L., Appelo, C.A.J., 1999. User's guide to PHREEQC (version 2) - a Computer Program for Speciation, batch-reaction, one-dimensional transport, and inverse geochemical calculations. USGS Report 99–4259.

Pelletier, B., 1996. Serpentines in Nickel Silicate Ore from New Caledonia, 6/96. Australasian Instituteof Mining and Metallurgy Publication Series - Nickel conference, Kalgoorlie, pp. 197–205 (Western Australia).

Pouchou, J.L., Pichoir, F., 1991. Quantitative analysis of homogeneous or stratified microvolumes applying the model "PAP". In: Heinrich, K.F.J., Newbury, D.E. (Eds.), Electron Probe Quantitation. Springer US, New York, pp. 31–75.

Putzolu, F., Abad, I., Balassone, G., Boni, M., Cappelletti, P., Graziano, S.F., Santoro, L., 2020a. Parent rock and climatic evolution control on the genesis of Ni-bearing clays in Ni-Co laterites: new inferences from the Wingellina deposit (Western Australia). Ore Geol. Rev. 120, 103431.

Putzolu, F., Abad, I., Balassone, G., Boni, M., Mondillo, N., 2020b. Ni-bearing smectites in the Wingellina laterite deposit (Western Australia) at nanoscale: TEM-HRTEM evidences of the formation mechanisms. Appl. Clay Sci. 196, 105753.

Roqué-Rosell, J., Mosselmans, J.F.W., Proenza, J.A., Labrador, M., Galí, S., Atkinson, K. D., Quinn, P.D., 2010. Sorption of Ni by "lithiophorite-asbolane" intermediates in Moa Bay lateritic deposits, eastern Cuba. Chem. Geol. 275, 9–18.

Roqué-Rosell, J., Villanova-de-Benavent, C., Proenza, J.A., 2017. The accumulation of Ni in serpentines and garnierites from the Falcondo Ni-laterite deposit (Dominican Republic) elucidated by means of µXAS. Geochem. Cosmochim. Acta 198, 48–69.

Saldi, G.D., Köhler, S.J., Marty, N., Oelkers, E.H., 2007. Dissolution rates of talc as a function of solution composition, pH and temperature. Geochem. Cosmochim. Acta 71, 3446–3457.

Santoro, L., Putzolu, F., Mondillo, N., Boni, M., Herrington, R., 2021. Trace element geochemistry of iron-(oxy)-hydroxides in Ni (Co)-laterites: review, new data and implications for ore forming processes. Ore Geol. Rev., 104501

Soler, J.M., Cama, J., Galí, S., Meléndez, W., Ramírez, A., Estanga, J., 2008. Composition and dissolution kinetics of garnierite from the Loma del Hierro Ni-laterite deposit. Venezuela. Chem. Geol. 249, 191–202.

Stoessell, R.K., 1988. 25 °C and 1 atm dissolution experiments of sepiolite and kerolite. Geochem. Cosmochim. Acta 52, 365–374.

Tauler, E., Lewis, J.F., Villanova-de-Benavent, C., Aiglsperger, T., Proenza, J.A., Domènech, C., Gallardo, T., Longo, F., Galí, S., 2017. Discovery of Ni-smectite rich saprolite at Loma Ortega, Falcondo mining district (Dominican Republic): geochemistry and mineralogy of an unusual case of "hybrid hydrous Mg silicate – clay silicate" type Ni-laterite. Miner. Deposita. https://doi.org/10.1007/s00126-017-0750-8.

Tauler, E., Proenza, J.A., Galí, S., Lewis, J., Labrador, M., García-Romero, E., 2009. Ni-sepiolite-falcondoite in garnierite mineralisation from the Falcondo Ni-laterite deposit, Dominican Republic. Clay Miner. 44, 435–454.

Trescases, J.J., 1973. Weathering and geochemical behaviour of the elements of ultramafic rocks in New Caledonia. In: Fisher, N.G. (Ed.), Metallogenic Provinces and Mineral Deposits in the Southwestern Pacific, vol. 141. Bureau of Mineral Resources, Department Minerals and Energy Bulletin, Canberra, pp. 149–161.

Villanova-de-Benavent, C., Proenza, J.A., Galí, S., García-Casco, A., Tauler, E., Lewis, J. F., Longo, F., 2014. Garnierites and garnierites: textures, mineralogy and geochemistry of garnierites in the Falcondo Ni-laterite deposit, Dominican Republic. Ore Geol. Rev. 58, 91–109.

Villanova-de-Benavent, C., Nieto, F., Viti, C., Proenza, J.A., Galí, S., Roqué-Rosell, J., 2016. Ni-phyllosilicates (garnierites) from the Falcondo Ni-laterite deposit (Dominican Republic): mineralogy, nanotextures and formation mechanisms by HRTEM and AEM. Am. Mineral. 101, 1460–1473.

Villanova-de-Benavent, C., Domènech, C., Tauler, E., Galí, S., Tassara, C.S., Proenza, J.A., 2017. Fe–Ni-bearing serpentines from the saprolite horizon of Caribbean Ni-laterite deposits: new insights from thermodynamic calculations. Miner. Deposita 52, 979–992.

Villanova-de-Benavent, C., Jawhari, T., Roqué-Rosell, J., Galí, S., Proenza, J.A., 2019. Ni-bearing phyllosilicates ("garnierites"): new insights from thermal analysis, µRaman and IR spectroscopy. Appl. Clay Sci. 175, 47–66.

Wells, M.A., Ramanaidou, E.R., Verrall, M., Tessarolo, C., 2009. Mineralogy and crystal chemistry of "garnierites" in the Goro lateritic nickel deposit, New Caledonia. Eur. J. Mineral 21, 467–483.